Journal of Power Sources 381 (2018) 18–25

Contents lists available at ScienceDirect

Journal of Power Sources

journal homepage: www.elsevier.com/locate/jpowsour

Rich-burn, flame-assisted fuel cell, quick-mix, lean-burn (RFQL) combustor and power generation

Ryan J. Milcarek*, Jeongmin Ahn

Department of Mechanical and Aerospace Engineering, Syracuse University, Syracuse, NY 13244-1240, USA

HIGHLIGHTS

- Novel rich-burn, flame-assisted fuel cell, quick-mix, lean-burn combustor proposed.
- An optimal fuel-lean equivalence ratio of 0.8 is observed for peak power density.
- Richer fuel-rich equivalence ratios increase the fuel cell power density and OCV.
- Flame-assisted fuel cell electrical efficiency improved from 0.144% to 0.358%.

ARTICLE INFO

Keywords:
Flame-assisted fuel cell (FFC)
Micro-combined heat and power
Micro-tubular solid oxide fuel cell (mT-SOFC)
Rich-burn quick-mix lean-burn (RQL) combustor
Two-stage combustor
Fuel-rich combustion

ABSTRACT

Micro-tubular flame-assisted fuel cells (mT-FFC) were recently proposed as a modified version of the direct flame fuel cell (DFFC) operating in a dual chamber configuration. In this work, a rich-burn, quick-mix, lean-burn (RQL) combustor is combined with a micro-tubular solid oxide fuel cell (mT-SOFC) stack to create a rich-burn, flame-assisted fuel cell, quick-mix, lean-burn (RFQL) combustor and power generation system. The system is tested for rapid startup and achieves peak power densities after only 35 min of testing. The mT-FFC power density and voltage are affected by changes in the fuel-lean and fuel-rich combustion equivalence ratio. Optimal mT-FFC performance favors high fuel-rich equivalence ratios and a fuel-lean combustion equivalence ratio around 0.80. The electrical efficiency increases by 150% by using an intermediate temperature cathode material and improving the insulation. The RFQL combustor and power generation system achieves rapid startup, a simplified balance of plant and may have applications for reduced NO_x formation and combined heat and power.

1. Introduction

Solid oxide fuel cells (SOFCs) are solid-state, electrochemical energy conversion devices that have the potential for high efficiency and high fuel flexibility, but in general have suffered from slow startup and limited on/off and thermal cycling [1]. Thermal cycling is more of a challenge in the Dual Chamber (DC-SOFC) [2,3] configuration, which prompted the Single Chamber (SC-SOFC) [4–6] and the Direct Flame Fuel Cell (DFFC) configurations [7]. DFFCs are SOFCs operating directly in a flame in a simple, no-chamber setup [7–30]. The advantages of direct operation in a flame with no chamber include rapid startup, rapid thermal cycling, high fuel flexibility, and simplifications to the thermal management and reforming systems [31]. Unfortunately, thermal gradients across the cell resulting from direct contact with flame, low power density and low electrical efficiency have been major challenges for DFFCs to date [19,22,32]. Despite the potential for improving rapid startup and cycling, DFFCs are still being investigated for improvements in these areas.

A recent change to the original DFFC occurred with the proposal of operating a micro-tubular SOFC (mT-SOFC) in a dual chamber configuration directly in the combustion exhaust, termed a micro-Tubular Flame-assisted Fuel Cell (mT-FFC) [31–34]. The dual chamber configuration changes the typical partially premixed combustion setup of the DFFC to a premixed system with better control over the final combustion equivalence ratio and exhaust composition [31]. The premixed combustion exhaust composition has been characterized for methane and propane fuels in previous studies and FFC performance based on a model combustion exhaust has been conducted [31,33,35]. A micro combined heat and power system design has been proposed for this technology [32,36]. However, the dual chamber configuration means that additional fuel remains after passing through the fuel cell because 100% fuel utilization is not possible as a result of Nernstian losses. To overcome this a second, fuel-lean combustion in the fuel cell downstream is necessary. To date only the first-stage combustion and fuel cell

* Corresponding author.
E-mail address: rjmilcar@syr.edu (R.J. Milcarek).

https://doi.org/10.1016/j.jpowsour.2018.02.006
Received 30 November 2017; Received in revised form 30 January 2018; Accepted 2 February 2018

operation in a model exhaust have been investigated, but a working system using this setup has not been developed.

The notion of a first-stage, fuel-rich combustion followed by a second-stage, fuel-lean combustion is an old combustor technology typically utilized to lower NO_x emissions from gas turbines with applications like jet engines [37–39]. The first-stage, fuel-rich combustion occurs at equivalence ratios above 1 which reduces the flame temperature and thereby reduces 'thermal NO_x' formation through the Zeldovich mechanism [40]. Reduction in 'fuel NO_x', or the oxidation of chemically bound nitrogen compounds in the fuel, has also been observed for two-stage combustion [40]. A premixed oxygen-deficient combustion, i.e. fuel-rich, leads to fuel bound nitrogen conversion to N_2 instead of complete conversion to NO which has been observed in oxygen-rich, i.e. fuel-lean, conditions [41,42]. The remaining fuel is then oxidized in a second-stage, fuel-lean combustor, but it requires a quick mixing of the oxidant stream in order to eliminate local high temperature regions and prevent further thermal NO_x formation [42]. As a result, this technology is often referred to as a Rich-burn, Quick-mix, Lean-burn (RQL) combustor, Rich-quench-lean (RQL) combustor [37,39,43,44] or two-stage combustor [40].

In this work, a new kind of two-stage RQL combustor is proposed. A first-stage, fuel-rich combustion is used to generate syngas in the exhaust stream. The exhaust then passes through SOFCs for conversion of the syngas to electrochemical power and thermal energy. Any remaining fuel existing in the fuel cell exhaust is mixed with an oxidant stream and a second-stage, fuel-lean combustion occurs. The first-stage, fuel-rich combustion provides thermal energy for the SOFC operation along with syngas while additional heat can be recovered from this stage and from the second-stage, fuel-lean combustion. This technology is denoted a Rich-burn, Flame-assisted fuel cell, Quick-mix, Lean-burn (RFQL) combustor. Fig. 1 shows one embodiment of the technology with a mT-SOFC stack arranged in a circle following the fuel-rich combustion chamber. This RFQL configuration operating on methane fuel is developed and investigated here.

2. Experimental setup

2.1. Combustor development and characterization

A RFQL combustor like the one shown in Fig. 1 was developed. A spark ignitor is used for ignition of the fuel/air mixture in the fuel-rich combustion chamber. K-type thermocouples are placed at different points of the fuel-rich and fuel-lean combustion chambers as shown in Fig. 2b. A flame arrestor is placed in the tubing before entering the

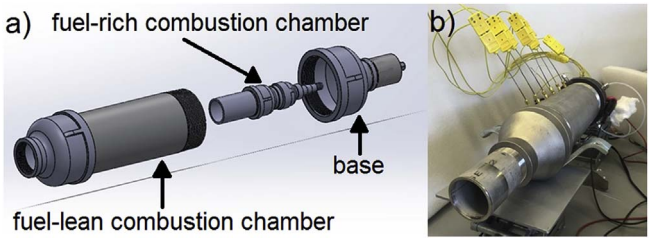

Fig. 2. a) Exploded view of the RFQL combustor CAD model showing the base with fuel-rich combustion chamber and fuel-lean combustion chamber and **b)** RFQL combustor assembled.

RFQL combustor in order to prevent flashback. Methane and air are regulated at different fuel/air equivalence ratios using mass flow controllers. For the fuel-rich combustion chamber, the equivalence ratio is regulated between 1.05 and 1.40. The methane flow rate is fixed while the air flow rate is adjusted to achieve the desired equivalence ratio. Different flow rates of methane are also investigated ranging from 1.0 to 2.4 L min^{-1}. The equivalence ratio (Ø) is defined in Eq. (1) below. Here n_{fuel} and n_{air} are the molar flow rates of fuel and air, respectively; and n^S_{fuel} and n^S_{air} are the molar flow rates required for stoichiometric combustion of fuel and air, respectively.

$$\varnothing = \frac{n_{fuel}/n_{air}}{n^S_{fuel}/n^S_{air}} \quad (1)$$

For fuel-rich combustion of methane and air, the following general reaction (2) occurs in the fuel-rich combustion chamber. Here a, b, c, and d are the mole fractions of the products of combustion. While the concentration of the products of combustion can vary significantly with the equivalence ratio (Ø), the species shown in Eq. (2) are the primary species observed in previous work [31,32] for the equivalence ratios investigated in this study.

$$\varnothing CH_4 + 2(O_2 + 3.76N_2) \rightarrow aCO + bCO_2 + cH_2 + dH_2O + 2(3.76)N_2 \quad (2)$$

For the second-stage, fuel-lean combustion, a mass flow controller is used to regulate the air flow. Four ports allow the air flow to be distributed evenly around the chamber. The air then passes over the outside of the fuel-rich combustion chamber for preheating. After preheating, the air passes over the SOFC stack for electrochemical reduction of the oxygen at the cathode. Any remaining fuel autoignites at the SOFC outlet for the second stage, fuel-lean combustion. The following reaction (3) occurs at the SOFC outlet.

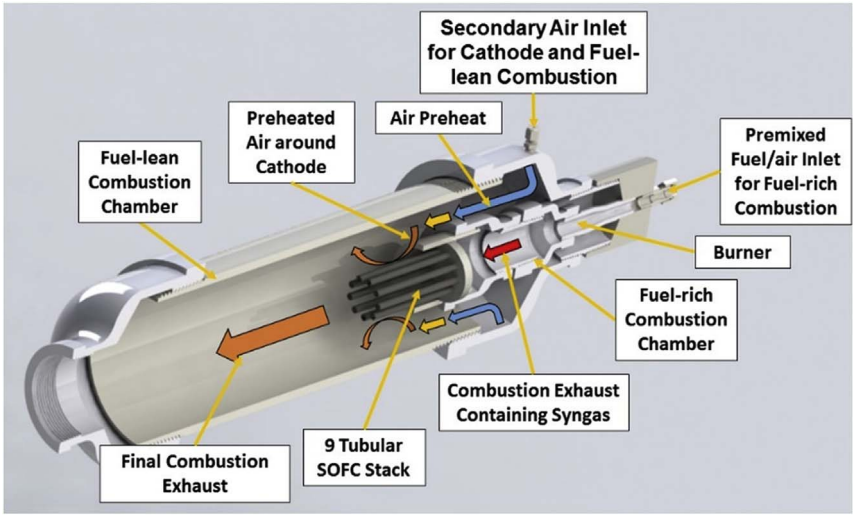

Fig. 1. One embodiment of the RFQL combustor with 9 mT-FFC stack.

Table 1
Methane and air flow rate for the fuel-rich combustion chamber and air for the fuel lean combustion chamber at different fuel-rich and fuel-lean equivalence ratios and fixed methane flow rate of 2.4 L min^{-1}

Fuel-rich combustion chamber			Fuel-lean combustion chamber air flow rate (L.min^{-1}) at different equivalence ratios					
Fuel-rich equivalence ratio	Methane flow rate (L.min^{-1})	Air flow rate (L.min^{-1})	0.90	0.85	0.80	0.75	0.70	0.65
1.05	2.4	21.7600	3.6267	5.1200	6.8000	8.7040	10.8800	13.3908
1.10	2.4	20.7709	4.6158	6.1091	7.7891	9.6931	11.8691	14.3799
1.15	2.4	19.8678	5.5188	7.0122	8.6922	10.5962	12.7722	15.2829
1.20	2.4	19.0400	6.3467	7.8400	9.5200	11.4240	13.6000	16.1108
1.25	2.4	18.2784	7.1083	8.6016	10.2816	12.1856	14.3616	16.8724
1.30	2.4	17.5754	7.8113	9.3046	10.9846	12.8886	15.0646	17.5754
1.35	2.4	16.9244	8.4622	9.9556	11.6356	13.5396	15.7156	18.2263
1.40	2.4	16.3200	9.0667	10.5600	12.2400	14.1440	16.3200	18.8308

$$H_2 + CO + O_2 \rightarrow CO_2 + H_2O \quad (3)$$

Air is supplied to the fuel-lean combustion chamber to ensure that the second-stage combustion results in a net fuel-lean combustion that is regulated between equivalence ratios of 0.65 and 0.90. The flow rates of methane and air for the fuel-rich combustion chamber and air for the fuel-lean combustion chamber are shown for the case of a methane flow rate of 2.4 L min^{-1} in Table 1. Similar calculations are used to determine the flow rates of air for different methane flow rates. LabVIEW software is used with National Instruments data acquisition interfaced with a computer for control of the mass flow controllers and monitoring of the temperatures. Combustion characterization of fuel-rich methane combustion was carried out previously and results are comparable in this setup [31–33]. As a result, combustion characterization is not repeated here.

2.2. Fuel cell fabrication and characterization

Micro-tubular SOFCs (mT-SOFCs) are fabricated as previously reported with a few details repeated here [31,32]. The anode is Ni + YSZ (yttria-stabilized zirconia) with YSZ electrolyte and an $(La_{0.8}Sr_{0.2})_{0.95}MnO_{3-x}$ (LSM) + YSZ cathode. Nine mT-SOFCs are connected in series to form the stack design as previously reported [34]. Silver paste was applied to the cathode and silver wire was wound around the cathode for current collection. Each fuel cell has an active area of 1.66 cm^2 for a total stack area of 14.94 cm^2. Current collection from the anode was conducted on the outside of the mT-SOFC with gold paste as described and depicted in previous work [34]. The fuel-rich combustion chamber has 9 circular ports (0.33 cm diameter) at the end through which all of the products of combustion flow. The diameter of the ports was slightly larger than the mT-SOFCs external diameter (0.32 cm), which allows the mT-SOFCs to be inserted into the ports. The mT-SOFCs were then sealed in place using ceramic paste. To further investigate the fuel cell performance, additional mT-SOFCs were fabricated with a $Sm_{0.20}Ce_{0.80}O_{2-X}$ (SDC) buffer layer [2,3] separating the YSZ electrolyte from an $(La_{0.60}Sr_{0.40})_{0.95}Co_{0.20}Fe_{0.80}O_{3-X}$ (LSCF) + SDC (7:3 w/w) cathode. The buffer layer was applied by wet powder spraying the SDC onto the mT-SOFC and was then dried and sintered at 1350 °C for 4 h. The LSCF + SDC cathode was then dip coated on top of the buffer layer, dried and sintered at 1100 °C for 4 h with an active area of 1.83 cm^2. A Keithley 2420 sourcemeter was interfaced with a computer for data acquisition. The current-voltage (IV) method with 4-probe technique was used to measure the stack polarization and power density. Two silver wires were connected to the cathode of the first mT-SOFC in the stack and two silver wires were connected to the anode of the last mT-SOFC in the stack for current and voltage measurements.

3. Results and discussion

In order to characterize the RFQL combustors baselines performance, a 9 mT-SOFC stack with LSM + YSZ cathode was tested before applying any insulation to the combustion chamber. The stack achieved an open circuit voltage (OCV) of 6 V and its highest performance (33 mW cm^{-2}) at an equivalence ratio of 1.05. In previous work in a dual chamber FFC setup at fixed temperatures [31,34], minimum OCV and minimum power density were predicted to occur at lower equivalence ratios due to a limited amount of fuel (i.e., syngas) in the exhaust stream. As the equivalence ratio increases above 1.20, the syngas concentration and especially H_2 concentration become more significant allowing less concentration losses in the fuel cell and better performance of the fuel cell. In this initial test the best performance occurred at lower equivalence ratios and decreased with increasing equivalence ratio. Changes in the temperature of the combustion chambers in this RFQL setup are important as the flame temperature, exhaust temperature and the air temperature around the cathode all decreased when the equivalence ratio increases. The air around the cathode had a very low temperature (635–656 °C) compared to normal operating temperatures for an LSM based cathode, which are typically above 800 °C [2]. Despite the increased syngas in the exhaust at higher equivalence ratios, the temperature plays a dominant role in fuel cell performance when no insulation is applied to the RFQL combustor. To enhance the fuel cell performance, the inner side of the fuel-lean combustion chamber was insulated. Open area around the burner, shown in Fig. 1, was also insulated to decrease possible heat losses. Adding the insulation to the fuel-lean combustion chamber increased the fuel-lean combustion chamber temperature from 635-656 °C to 765–785 °C at the same flow rates of methane and air of the initial test. A 9 cell mT-SOFC was tested in a furnace with H_2 fuel at a total flow rate of 450 mL min^{-1} to establish a baseline for the stacks performance. Since the cathode air temperatures increased to 765–785 °C with insulation, the stack was tested in H_2 at 700 °C, 750 °C and 800 °C. At a stack voltage of 5.4 V (0.6 V per cell), power densities of 118, 130, and 250 mW cm^{-2} were achieved at 700 °C, 750 °C and 800 °C, respectively with pure H_2.

The stack was then sealed to the RFQL combustor and methane was ignited at an equivalence ratio of 1.2. The Keithley 2420 was initiated just after igniting the methane to monitor the fuel cell voltage during startup. Fig. 3a shows the fuel cell voltage during startup. The stack reached a stable operating voltage around 7.5 V after ~4 min of testing. The anode temperature was over 950 °C in less than 4 min. However, the temperature in the fuel-lean combustion chamber increased quickly in the first 12 min and then slowly afterward. After 12 min the temperature around the cathode was 626 °C. After 30 min of testing the temperature in the fuel-lean combustion chamber began to stabilize around 750 °C and the first polarization curve was taken after 35 min as shown in Fig. 3b. The peak power density of ~128 mW cm^{-2} was the highest power density achieved with LSM cathode at an equivalence ratio of 1.25 and occurred after only 35 min of startup. With better thermal management, the fuel-lean combustion chamber could be brought to operating temperature faster resulting in more rapid startup

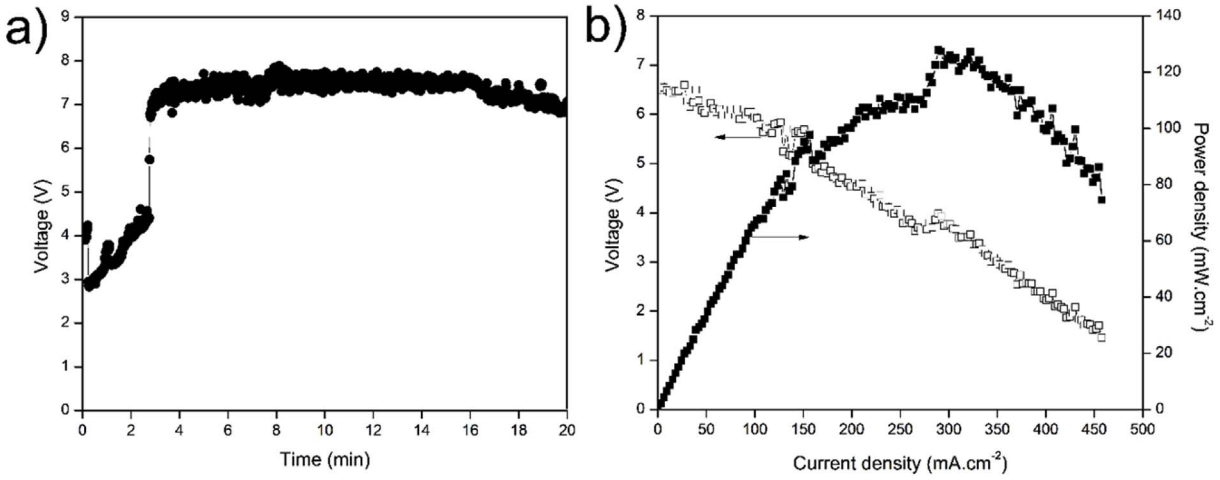

Fig. 3. mT-FFC stack **a)** voltage after starting up and **b)** first test conducted 35 min after startup at an equivalence ratio of 1.25.

and testing than reported here.

Before investigating the effect of the fuel-rich equivalence ratio on the mT-FFC stack performance, the fuel-lean combustion equivalence ratio was varied and the fuel-rich combustion equivalence ratio was fixed at 1.30 and 1.40 with methane flowrate fixed at 2.4 L min^{-1}. Fig. 4 shows the results. Fig. 4a shows the changes in polarization for different fuel-lean combustion equivalence ratios from 0.65 to 0.90 with the fuel-rich combustion equivalence ratio fixed at 1.30 while Fig. 4b shows similar results for a fuel-rich combustion equilvalence ratio of 1.40. From Fig. 4a and b, there was not significant variation in the polarization or power density with change in the fuel-lean equivalence ratio. A closer examination of the power density at a FFC stack voltage of 5.4 V (0.6 V per cell) and OCV with varying fuel-lean equivalence ratio is shown in Fig. 4c. The power density at 0.6 V per cell varied by less than 13%, but a peak in the power density was observed at an fuel-lean combustion chamber equivalence ratio of 0.8. This result occurred for a fuel-rich combustion equivalence ratio of 1.3 and 1.4. The reason for the optimal appears to be due to the impact of

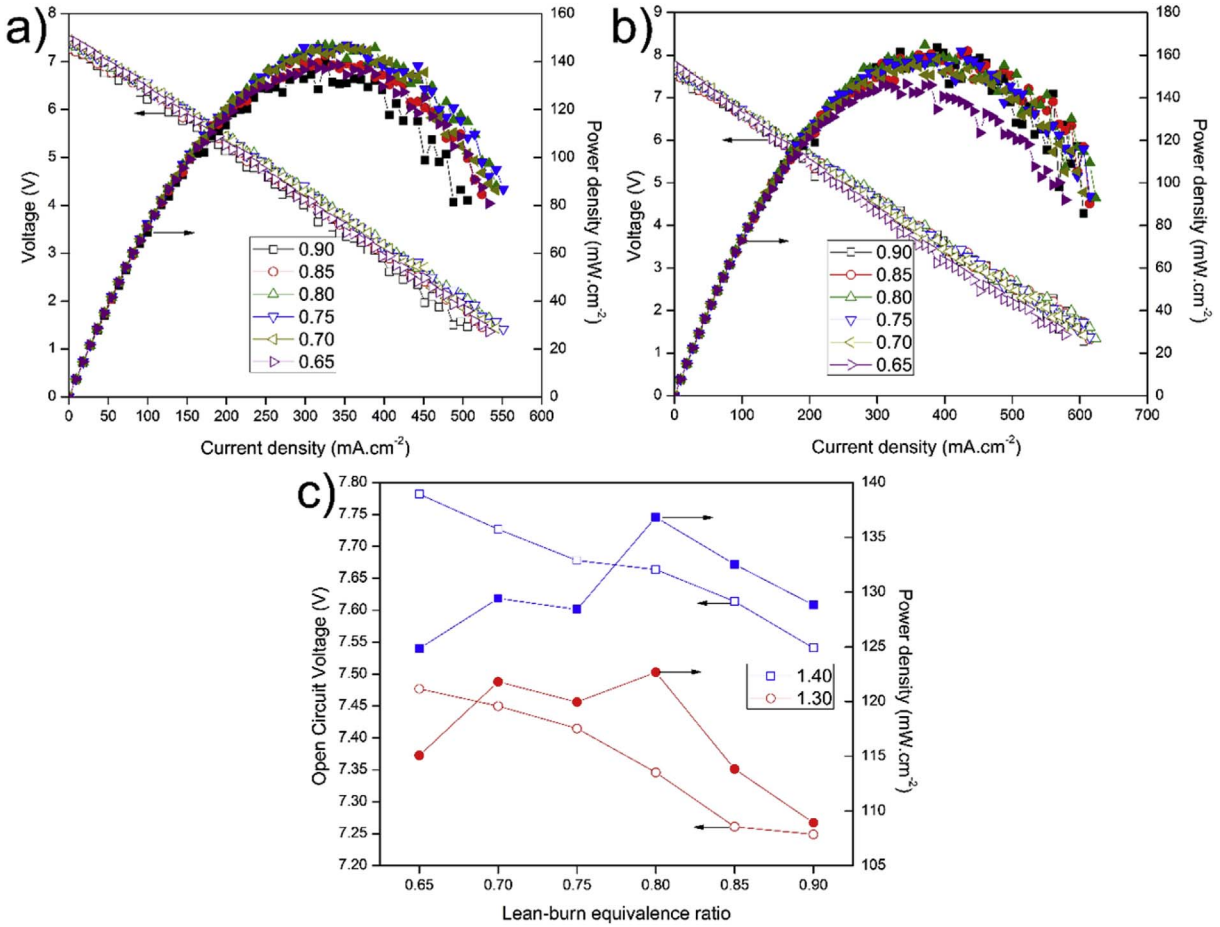

Fig. 4. mT-FFC stack polarization and power density with varying fuel-lean combustion chamber equivalence ratio between 0.65 and 0.90 and with fixed fuel-rich combustion equivalence ratio of **a)** 1.30 and **b)** 1.40 and **c)** a summary of results at 0.6 V per cell.

temperature and decreased polarization in the fuel cell. As the fuel-lean equivalence ratio is decreased from 0.9 to 0.65, the air flow rate to the fuel-lean combustion chamber increases as shown in Table 1 and results in a decrease in the air temperature around the cathode. This was confirmed with thermocouples and by monitoring the stack OCV as shown in Fig. 4c. The fuel cell OCV is well known to increase with decreasing temperature. The decreasing temperature also has a negative impact on the electrode kinectics resulting in decreased performance, as shown from an equivalence ratio of 0.8 to 0.65. However, the increase in air flow rate also increases the amount of O_2 available to the cathode which appears to be responsible for the initial increase in performance as the fuel-lean combustion equivalence ratio decreases from 0.9 to 0.8. An optimal fuel-lean equivalence ratio at 0.8 results.

With an optimal fuel-lean equivalence ratio uncovered for the RFQL combustor, the fuel-lean equivalence ratio was fixed and the fuel-rich equivalence ratio was increased from 1.05 until reaching an upper flammability limit for the apparatus at 1.4. The upper flammability limit is the highest fuel-rich equivalence ratio achieved for a gas phase reaction and is notably fuel and apparatus dependent as described in other work [45,46]. The mT-FFC stack polarization and power density at equivalence ratios from 1.05 to 1.4 is shown in Fig. 5. As shown, the stack OCV and power density increase significantly with increasing fuel-rich equivalence ratio. The increased OCV and power density are a result of increased sygnas concentration in the exhaust which was previously shown to increase from a mole percentage of only 1.4% at an equivalence ratio of 1.05 up to 21.2% at an equivalence ratio of 1.4 [32,33]. Methane and other hydrocarbons were not detected in fuel-rich combustion exhaust in that work indicating that the mT-FFCs in the RFQL combustor has electrochemical reactions from syngas only according to the following half reactions (4) and (5).

$$H_2 + O^{2-} \rightarrow H_2O + 2e^- \quad (4)$$

$$CO + O^{2-} \rightarrow CO_2 + 2e^- \quad (5)$$

In addition, the presense of water vapor in the exhuast makes the water-gas shift reaction a possibility for indirect use of CO according to the following reaction (6).

$$CO + H_2O \rightarrow CO_2 + H_2 \quad (6)$$

The primary fuel for the mT-FFC is syngas, the concentration of which is highly dependent on the equivalence ratio. The trends for the polarization and power density curves at increasing equivalence ratios were predicted previously using a model combustion exhaust based on the exhaust composition at various fuel-rich combustion equivalence ratios [31,32,34]. The results here confirm the previous predictions, although the change of temperature with equivalence ratio is important in the RFQL combustor and was not considered in previous studies. The results in Fig. 5 differ signifcantly from the test without insulation due to the temperature increase of the air around the cathode with the added insulation. At a mT-FFC stack operating voltage of 5.4 V (0.6 V per cell) the power density was 120 mW cm^{-2} at an equivalence ratio of 1.4. This power density, which occurred with the air temperature around the cathode at 776 °C, is nearly half of the power density obtained with H_2 at 800 °C, is nearly the same as the stacks power density at 750 °C with H_2 and is an improvement of nearly 4 times compared to the initial test without insulation. Obtaining peak performance in the RFQL combustor is highly dependent on proper thermal management.

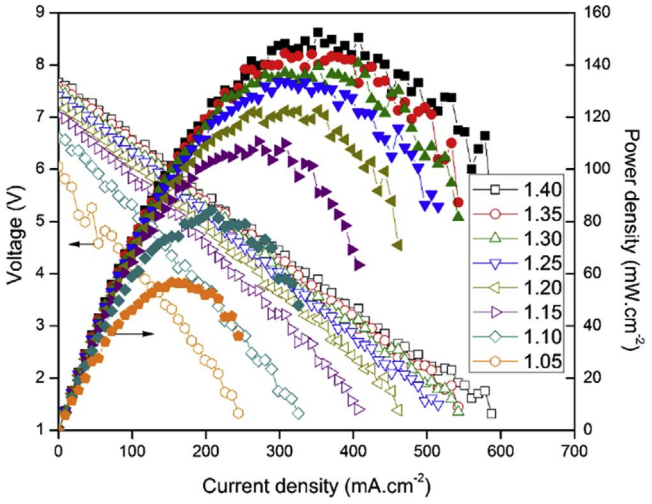

Fig. 5. mT-FFC stack polarization and power density with fixed fuel-lean combustion equilvalence raito of 0.8 and varying fuel-rich combustion equivalence ratio from 1.05 to 1.40.

Despite the improved performance, the electrical efficiency of RFQL combustor remained low. To assess the possibility of increasing the electrical efficiency, the methane flow rate was decreased from 2.4 to 1.6 L min^{-1} while fixing the fuel-rich and fuel-lean equivalence ratios at 1.25 and 0.8, respectively. Electrical efficiency (ε) is defined based on a previously reported method [19] shown in Eq. (7).

$$\varepsilon = \frac{Electric\ power\ generated\ by\ FFC}{Heating\ power\ of\ fuel} = \frac{P \cdot A \cdot V_m}{\dot{V} \cdot HHV} \quad (7)$$

Here, P is the mT-FFC peak power density, A the total fuel cell active area, V_m is the molar volume at standard conditions (2.24×10^{-2} m^{3}mol^{-1}), $\dot{V}$ is the methane flow rate at standard conditions and HHV is the higher heating value of methane (8.89×10^5 J mol^{-1}). The polarization and power density results are shown in Fig. 6a. As shown, the power density decreased with decreasing methane flow rate. However, the electrical efficiency did improve slightly as shown in Fig. 6b. The main reason for the decreased performance and only slight increase (~5%) in electrical efficiency despite fixed equivalence ratios is the decrease in heat release and the resulting decrease in air temperature around the cathode as shown in Fig. 6b.

The air temperature around the cathode (730–790 °C) significantly affected the FFC performance in this setup while the temperature of the exhaust gases passing over the anode were over 900 °C. The anode exhaust gas temperatures are appropriate for the Ni + YSZ anode and YSZ electrolyte chosen for this setup, while the LSM + YSZ cathode is operating at the low end of its temperature range. Decreasing the flow rate of methane to improve efficiency only resulted in slight improvements in efficiency because of the rapid decrease in cathode air temperature. Due to the intermediate temperature range of the cathode air and a higher anode temperature achieved in the RFQL combustor, a LSCF + SDC cathode was applied with an SDC buffer layer onto the YSZ electrolyte with Ni + YSZ anode. A cross-sectional image obtained from a scanning electron microscope is included in Fig. A.1 in the appendix. The insulation was also improved further with an ultra-low thermal conductivity (0.044 W m^{-1} K^{-1} at 800 °C) insulation. Nine mT-SOFCs were then sealed to the RFQL combustor and tested at methane flow rates of 1.0–1.6 L min^{-1}, which were lower than the flow rates investigated in Fig. 6. For this test only one mT-FFC was tested at the top of the stack to assess peak power without any influence of stack related losses. The fuel-lean combustion equivalence ratio was again fixed at 0.80 while the fuel-rich combustion equivalence ratio was varied from 1.2 to 1.4. The polarization and power density are shown in Fig. 7. Similar trends of increasing OCV and power density with fuel-rich equivalence ratio were observed except the mT-FFC with LSCF + SDC cathode had much higher power density. At an equivalence ratio of 1.4 and methane flow rate of 1.6 L min^{-1} the FFC achieved a peak power density of 199 mW cm^{-2} and a power density of 184 mW cm^{-2} at 0.6 V. The power density did decrease as the methane flow rate decreased as shown in Fig. 7b–d, but the decrease in power density was less significant than in Fig. 6. For example, at a methane flow rate of 1.6, 1.4, 1.2 and 1.0 L min^{-1} the FFC power density at an operating voltage of 0.6 V was 184, 178, 161, and 125 mW cm^{-2}, respectively. These power densities were obtained at the highest equivalence ratios sustained at

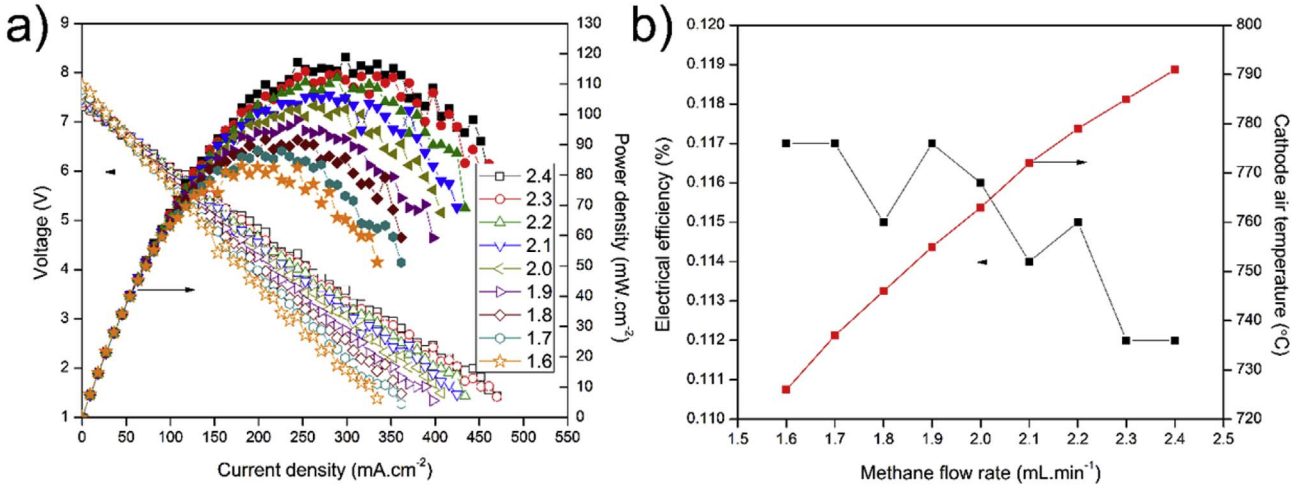

Fig. 6. a) mT-FFC stack polarization and power density with fixed fuel-rich (1.25) and fuel-lean (0.8) combustion equivalence ratios and varying methane flow rate 1.6–2.4 L min^{-1} and **b)** electrical efficiency and temperature change with methane flow rate.

each flow rate. As shown in Fig. 7, the highest equivalence ratio decreased from 1.4 to 1.375 as the flow rate decreased because of the decreased heat release with decreasing fuel flow rate and subsequent quenching of the flame.

The mT-FFC electrical efficiency with the LSCF + SDC cathode was calculated using Eq. (5) at a fuel-rich equivalence ratio of 1.25 and methane flow rates from 1.0 to 1.6 L min^{-1}. The results are plotted in Fig. 8a with the measured cathode air temperature at each condition. The trends are similar to those obtained for the mT-FFC with LSM + YSZ cathode test, but the increase in electrical efficiency was much more significant (~38% increase compared to ~5%). Despite the increase in electrical efficiency with decreasing methane flow rate, the electrical efficiency began to decrease again after reaching an optimal condition at a methane flow rate of 1.2 L min^{-1}. This optimal is due to the rapid decrease in cathode air temperature (740 °C down to 699 °C) when the methane flow rate decreased below 1.2 L min^{-1}. An electrical

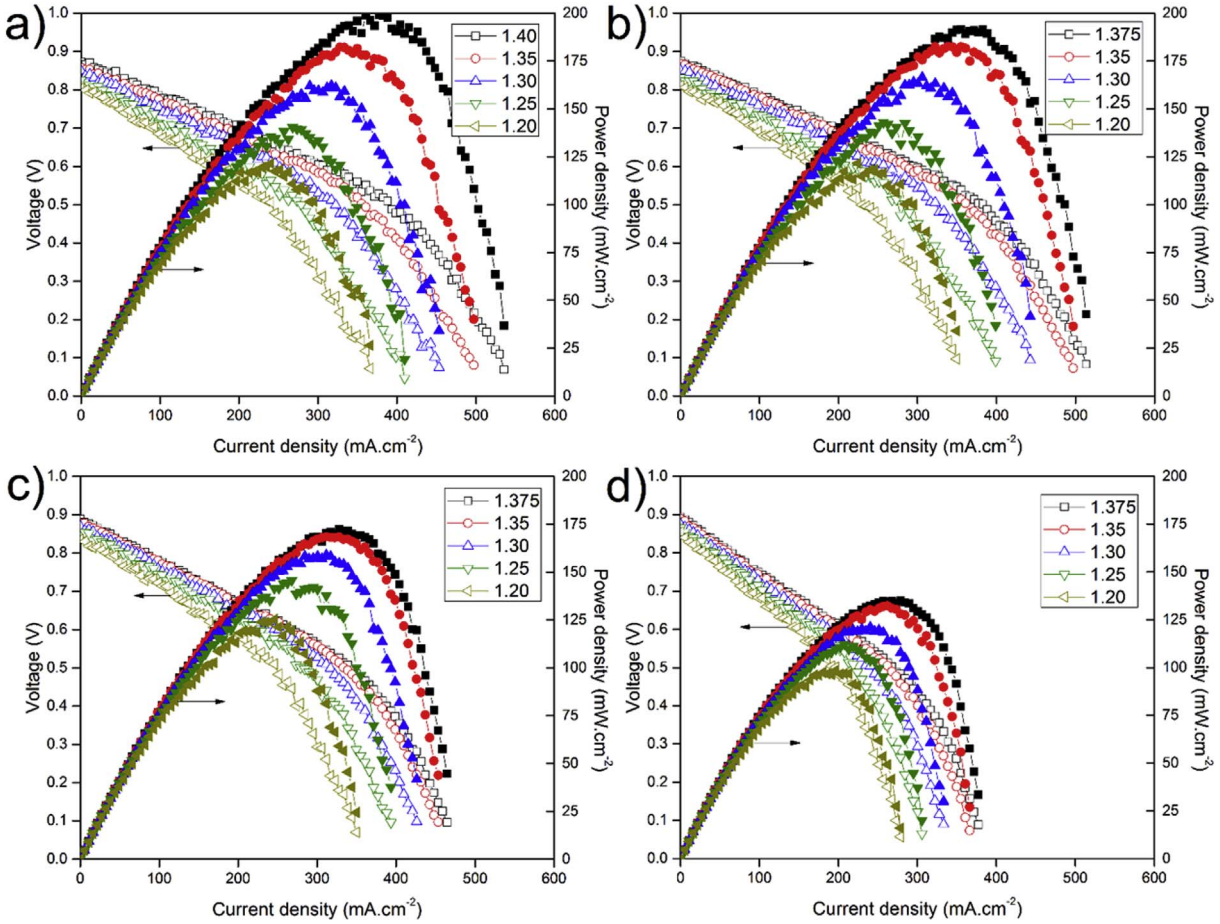

Fig. 7. mT-FFC polarization and power density with SDC + LSCF cathode for fuel-rich equivalence ratios of 1.2–1.4 and methane flow rates of **a)** 1.6 L min^{-1}, **b)** 1.4 L min^{-1}, **c)** 1.2 L min^{-1}, and **d)** 1.0 L min^{-1}.

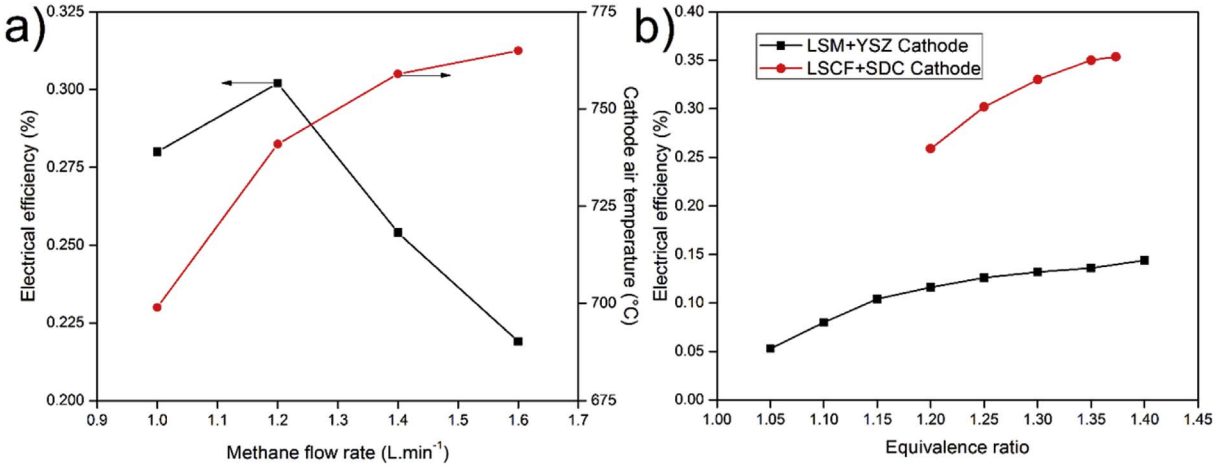

Fig. 8. a) SDC + LSCF cathode mT-FFC electrical efficiency and cathode air temperature with fixed fuel-lean combustion equilvalence ratio (0.8), fixed fuel-rich equivalence ratio (1.25) and varying methane flow rate 1.0–1.6 L min^{-1} and **b)** electrical efficiency comparison between LSCF + SDC cathode (methane flow rate 1.2 L min^{-1}) with LSM + YSZ cathode (methane flow rate 2.4 L min^{-1}).

efficiency comparison was conducted with the FFC having LSM + YSZ cathode and LSCF + SDC cathode at fuel-rich equivalence ratios from 1.05 to 1.40. The comparison is shown in Fig. 8b. The mT-FFC electrical efficiency, with LSCF + SDC cathode at the optimal methane flow rate (1.2 L min^{-1}) and fuel-rich equivalence ratio of 1.375, increased by 149% (up to 0.358%) compared to the mT-FFC with LSM + YSZ cathode at equivalence ratio 1.4 (methane flow rate of 2.4 L min^{-1}, electrical efficiency 0.144%). This increase is due to the LSCF + SDC cathode which is more suited to the operating conditions achieved in the RFQL combustor and the improved insulation. One previous study with methane fuel in a DFFC reported an optimal electrical efficiency of 0.19% [19]. While the improvement in electrical efficiency is significant compared to mT-FFC with LSM + YSZ cathode and is among the highest reported electrical efficiencies achieved for a DFFC or FFC [22], more work is needed to improve the electrical efficiency further. However, the RFQL combustor has significant potential for combined heat and power (CHP) applications because all of the fuel is reacted in the two-stage combustor and heat can easily be transferred from the fuel-lean combustion chamber to heat water or air. As a result, the combined efficiency is expected to be high.

While soot formation is a concern in DFFC and FFC research, the equivalence ratios tested in this study are below the critical equivalence ratio for soot formation from methane fuel [46]. As a result, soot formation is typically not observed under these conditions and it was not observed on the anode or combustion chamber in this study either.

4. Conclusions

The development of a dual chamber FFC configuration has been discussed in previous work and modeled with experiments and theory. The first self-sustained FFC is tested in a novel Rich-burn, Quick-mix, Lean-burn (RQL) combustor to make the first Rich-burn, Flame-assisted fuel cell, Quick-mix, Lean-burn (RFQL) combustor in this study. In short, the RFQL combustor is a two-stage combustor with mT-SOFCs between the fuel-rich combustion zone and the quick-mix, fuel-lean combustion zone. Combustion characteristic and heat release in the fuel-rich and fuel-lean combustion chambers impact the mT-SOFCs performance. The RFQL combustor shows potential for rapid startup, achieving a high OCV within 4 min. With a better thermal management to increase the fuel-lean combustion chamber temperature faster, a faster startup may be possible. The RFQL combustor shows optimal conditions for the fuel-lean combustion at an equivalence ratio of 0.80. This result is due to a balance between decreasing cathode air temperature at leaner fuel-lean (0.65–0.75) equivalence ratios and decreased O_2 for the cathode at less fuel-lean (0.85–0.9) equivalence ratios. Peak power density and electrical efficiency are found at richer fuel-rich equivalence ratios where there is greater syngas concentration in the exhaust. Soot formation was not observed in this study and only syngas fuel was found in the exhaust in previous work indicating potential for the RFQL combustor to operate directly with hydrocarbon fuels while limiting carbon deposition. A significant temperature difference between the anode and cathode of the mT-SOFC was observed. Lower temperature cathode materials better suited to the lower temperatures in the fuel-lean combustion chamber and better insulation were found to have a significant impact on the power generation and electrical efficiency. Applications in areas were RQL combustors are already utilized, like jet engines, in CHP applications or in various combined cycles power plants is possible.

Acknowledgement

This material is based upon work supported by an Agreement with Syracuse University awarded by its Syracuse Center of Excellence for Environmental and Energy Systems with funding under prime award number DE-EE0006031 from the U.S. Department of Energy and matching funding under award number 53367 from the New York State Energy Research and Development Authority (NYSERDA); from NYSERDA contract 61736; and by NEXUS-NY. This material is also based upon work supported by the National Science Foundation Graduate Research Fellowship Program under Grant No. 1746928. A related U.S. provisional patent application No. 62/551,961 was filed.

Appendix A. Supplementary data

Supplementary data related to this article can be found at http://dx.doi.org/10.1016/j.jpowsour.2018.02.006.

References

[1] W. Bujalski, C.M. Dikwal, K. Kendall, Cycling of three solid oxide fuel cell types, J. Power Sources 171 (2007) 96–100, http://dx.doi.org/10.1016/j.jpowsour.2007.01.029.
[2] R.J. Milcarek, K. Wang, M.J. Garrett, J. Ahn, Performance investigation of dual layer yttria-stabilized zirconia–samaria-doped ceria electrolyte for intermediate temperature solid oxide fuel cells, J. Electrochem. Energy Convers. Storage 13 (2016) 11002, http://dx.doi.org/10.1115/1.4032708.
[3] R.J. Milcarek, K. Wang, R.L. Falkenstein-Smith, J. Ahn, Performance variation with SDC buffer layer thickness, Int. J. Hydrogen Energy 41 (2016) 9500–9506, http://dx.doi.org/10.1016/j.ijhydene.2016.04.113.
[4] I. Riess, On the Single chamber solid oxide fuel cells, J. Power Sources 175 (2008) 325–337, http://dx.doi.org/10.1016/j.jpowsour.2007.09.041.

[5] I. Riess, P.J. van der Put, J. Schoonman, Solid oxide fuel cells operating on uniform mixtures of fuel and air, Solid State Ionics 82 (1995) 1–4, http://dx.doi.org/10.1016/0167-2738(95)00210-W.
[6] S. Raz, M.J.G. Jak, J. Schoonman, I. Riess, Supported mixed-gas fuel cells, Solid State Ionics 149 (2002) 335–341.
[7] M. Horiuchi, S. Suganuma, M. Watanabe, Electrochemical power generation directly from combustion flame of gases, liquids, and solids, J. Electrochem. Soc. 151 (2004) A1402, http://dx.doi.org/10.1149/1.1778168.
[8] H. Kronemayer, D. Barzan, M. Horiuchi, S. Suganuma, Y. Tokutake, C. Schulz, W.G. Bessler, A direct-flame solid oxide fuel cell (DFFC) operated on methane, propane, and butane, J. Power Sources 166 (2007) 120–126, http://dx.doi.org/10.1016/j.jpowsour.2006.12.074.
[9] M. Vogler, M. Horiuchi, W.G. Bessler, Modeling, simulation and optimization of a No-Chamber solid oxide fuel cell operated with a flat-flame burner, J. Power Sources 195 (2010) 7067–7077, http://dx.doi.org/10.1016/j.jpowsour.2010.04.030.
[10] M.M. Hossain, J. Myung, R. Lan, M. Cassidy, I. Burns, S. Tao, J.T.S. Irvine, Study on direct flame solid oxide fuel cell using flat burner and ethylene flame, ECS Trans. 68 (2015) 1989–1999, http://dx.doi.org/10.1149/06801.1989ecst.
[11] L. Sun, Y. Hao, C. Zhang, R. Ran, Z. Shao, Coking-free direct-methanol-flame fuel cell with traditional nickel-cermet anode, Int. J. Hydrogen Energy 35 (2010) 7971–7981, http://dx.doi.org/10.1016/j.ijhydene.2010.05.048.
[12] X. Zhu, B. Wei, Z. Lü, L. Yang, X. Huang, Y. Zhang, M. Liu, A direct flame solid oxide fuel cell for potential combined heat and power generation, Int. J. Hydrogen Energy 37 (2012) 8621–8629, http://dx.doi.org/10.1016/j.ijhydene.2012.02.161.
[13] Y. Wang, L. Sun, L. Luo, Y. Wu, L. Liu, J. Shi, The study of portable direct-flame solid oxide fuel cell (DF-SOFC) stack with butane fuel, J. Fuel Chem. Technol. 42 (2014) 1135–1139, http://dx.doi.org/10.1016/S1872-5813(14)60045-1.
[14] Y. Wang, Y. Shi, M. Ni, N. Cai, A micro tri-generation system based on direct flame fuel cells for residential applications, Int. J. Hydrogen Energy 39 (2014) 5996–6005, http://dx.doi.org/10.1016/j.ijhydene.2014.01.183.
[15] S. Endo, Y. Nakamura, Power generation properties of direct flame fuel cell (DFFC), J. Phys. Conf. Ser. 557 (2014) 12119, http://dx.doi.org/10.1088/1742-6596/557/1/012119.
[16] K. Wang, R. Ran, Y. Hao, Z. Shao, W. Jin, N. Xu, A high-performance No-Chamber fuel cell operated on ethanol flame, J. Power Sources 177 (2008) 33–39, http://dx.doi.org/10.1016/j.jpowsour.2007.11.004.
[17] Y. Wang, Y. Shi, X. Yu, N. Cai, J. Qian, S. Wang, Experimental characterization of a direct methane flame solid oxide fuel cell power generation unit, J. Electrochem. Soc. 161 (2014) F1348–F1353, http://dx.doi.org/10.1149/2.0381414jes.
[18] Y. Wang, Y. Shi, X. Yu, N. Cai, Thermal shock resistance and failure probability analysis on solid oxide electrolyte direct flame fuel cells, J. Power Sources 255 (2014) 377–386, http://dx.doi.org/10.1016/j.jpowsour.2014.01.035.
[19] K. Wang, R.J. Milcarek, P. Zeng, J. Ahn, Flame-assisted fuel cells running methane, Int. J. Hydrogen Energy 40 (2015) 4659–4665, http://dx.doi.org/10.1016/j.ijhydene.2015.01.128.
[20] M. Vogler, D. Barzan, H. Kronemayer, C. Schulz, M. Horiuchi, S. Suganuma, Y. Tokutake, J. Warnatz, W.G. Bessler, Direct-flame solid-oxide fuel cell (DFFC): a thermally self-sustained, air self- breathing, hydrocarbon-operated SOFC system in a simple, No-Chamber setup, ECS Trans. ECS, 2007, pp. 555–564 https://doi.org/10.1149/1.2729136.
[21] X. Zhu, Z. Lu¨, B. Wei, X. Huang, Z. Wang, W. Su, Direct flame SOFCs with $La_{0.75}Sr_{0.25}Cr_{0.5}Mn_{0.5}O_{3-\delta}$/Ni coimpregnated yttria-stabilized zirconia anodes operated on liquefied petroleum gas flame, J. Electrochem. Soc. 157 (2010) B1838, http://dx.doi.org/10.1149/1.3500976.
[22] K. Wang, P. Zeng, J. Ahn, High performance direct flame fuel cell using a propane flame, Proc. Combust. Inst. 33 (2011) 3431–3437, http://dx.doi.org/10.1016/j.proci.2010.07.047.
[23] Y.Q. Wang, Y.X. Shi, X.K. Yu, N.S. Cai, S.Q. Li, Integration of solid oxide fuel cells with multi-element diffusion flame burners, J. Electrochem. Soc. 160 (2013) F1241–F1244, http://dx.doi.org/10.1149/2.051311jes.
[24] T. Hirasawa, S. Kato, A study on energy conversion efficiency of direct flame fuel cell supported by clustered diffusion microflames, J. Phys. Conf. Ser. 557 (2014) 12120, http://dx.doi.org/10.1088/1742-6596/557/1/012120.
[25] Y. Wang, Y. Shi, N. Cai, X. Ye, S. Wang, Performance characteristics of a micro-tubular solid oxide fuel cell operated with a fuel-rich methane flame, ECS Trans. 68 (2015) 2237–2243, http://dx.doi.org/10.1149/06801.2237ecst.
[26] Y. Nakamura, S. Endo, Power generation performance of direct flame fuel cell (DFFC) impinged by small jet flames, J. Micromech. Microeng.Microeng. 25 (2015) 104015, , http://dx.doi.org/10.1088/0960-1317/25/10/104015.
[27] Y. Wang, H. Zeng, T. Cao, Y. Shi, N. Cai, X. Ye, S. Wang, Start-up and operation characteristics of a flame fuel cell unit, Appl. Energy 178 (2016) 415–421, http://dx.doi.org/10.1016/j.apenergy.2016.06.067.
[28] Y. Wang, H. Zeng, Y. Shi, T. Cao, N. Cai, X. Ye, S. Wang, Power and heat Co-Generation by micro-tubular flame fuel cell on a porous media burner, Energy 109 (2016) 117–123, http://dx.doi.org/10.1016/j.energy.2016.04.095.
[29] M.C. Tucker, A.S. Ying, Metal-supported solid oxide fuel cells operated in direct-flame configuration, Int. J. Hydrogen Energy 42 (2017) 24426–24434, http://dx.doi.org/10.1016/j.ijhydene.2017.07.224.
[30] H. Zeng, Y. Wang, Y. Shi, N. Cai, Biogas-fueled flame fuel cell for micro-combined heat and power system, Energy Convers. Manag. 148 (2017) 701–707, http://dx.doi.org/10.1016/j.enconman.2017.06.039.
[31] R.J. Milcarek, M.J. Garrett, K. Wang, J. Ahn, Micro-tubular flame-assisted fuel cells running methane, Int. J. Hydrogen Energy 41 (2016) 20670–20679, http://dx.doi.org/10.1016/j.ijhydene.2016.08.155.
[32] R.J. Milcarek, K. Wang, R.L. Falkenstein-Smith, J. Ahn, Micro-tubular flame-assisted fuel cells for micro-combined heat and power systems, J. Power Sources 306 (2016) 148–151, http://dx.doi.org/10.1016/j.jpowsour.2015.12.018.
[33] R.J. Milcarek, M.J. Garrett, A. Baskaran, J. Ahn, Combustion characterization and model fuel development for micro-tubular flame-assisted fuel cells, J. Vis. Exp. (2016) e54638, , http://dx.doi.org/10.3791/54638.
[34] R.J. Milcarek, M.J. Garrett, J. Ahn, Micro-tubular flame-assisted fuel cell stacks, Int. J. Hydrogen Energy 41 (2016) 21489–21496, http://dx.doi.org/10.1016/j.ijhydene.2016.09.005.
[35] R.J. Milcarek, M.J. Garrett, J. Ahn, Micro-tubular flame-assisted fuel cells, J. Fluid Sci. Technol. 12 (2017), http://dx.doi.org/10.1299/jfst.2017jfst0021 JFST0021-JFST0021.
[36] R.J. Milcarek, J. Ahn, J. Zhang, Review and analysis of fuel cell-based, micro-co-generation for residential applications: current state and future opportunities, Sci. Technol. Built Environ. 23 (2017) 1224–1243, http://dx.doi.org/10.1080/23744731.2017.1296301.
[37] A.S. Feitelberg, M.A. Lacey, The GE rich-quench-lean gas turbine combustor, J. Eng. Gas Turbines Power 120 (1998) 502, http://dx.doi.org/10.1115/1.2818173.
[38] P. Sampath, T.C.J. Hu, H. Ozem, Combustion technology challenges for small aviation gas turbines, 23rd Int. Congr. Aeronaut. Sci. 2002, pp. 1–22.
[39] S. Samuelsen, Rich burn, quick-mix, lean burn (RQL) combustor, NETL Handb. 1990, pp. 227–233.
[40] A.F. Sarofim, R.C. Flagan, NOx control for stationary combustion sources, Prog. Energy Combust. Sci. 2 (1976) 1–25, http://dx.doi.org/10.1016/0360-1285(76)90006-X.
[41] B.A. Folsom, C.W. Courtney, M.P. Heap, The effects of LBG composition and combustor characteristics on fuel NOx formation, J. Eng. Power 102 (1980) 459–467.
[42] D.L. Straub, K.H. Casleton, R.E. Lewis, T.G. Sidwell, D.J. Maloney, G.A. Richards, Assessment of rich-burn, quick-mix, lean-burn trapped vortex combustor for stationary gas turbines, J. Eng. Gas Turbines Power 127 (2005) 36, http://dx.doi.org/10.1115/1.1789152.
[43] C. Peterson, A. Sowa, G. Samuelsen, Performance of a Model Rich Burn-quick Mix-lean Burn Combustor at Elevated Temperature and Pressure, NASA/CR-2002-211992 (2002), pp. 1–90.
[44] J. Hosoi, N. Hiromitsu, D. Riechelmann, A. Fujii, J. Sato, Simple low NOx combustor technology, IHI Eng. Rev. 41 (2008) 46–50.
[45] S.R. Turns, An Introduction to Combustion: Concepts and Applications, second ed., McGraw-Hill, New York, 2000.
[46] I. Glassman, R.A. Yetter, N.G. Glumac, Combustion, fourth ed., Academic Press, Waltham, MA, 2015.

GLOSSARY

A: Fuel cell area
CHP: Combined heat and power
DC-SOFC: Dual chamber solid oxide fuel cell
DFFC: Direct flame fuel cell
FFC: Flame-assisted fuel cell
HHV: Higher heating value
LSCF: Lanthanum strontium cobalt ferrite
LSM: Lanthanum strontium manganite
mT-FFC: micro-tubular flame-assisted fuel cell
mT-SOFC: micro-tubular solid oxide fuel cell
n_{air}: Molar flow rates of air
n_{fuel}: Molar flow rates of fuel
n_{air}^{S}: Molar flow rates of air for stoichiometric combustion
n_{fuel}^{S}: Molar flow rates of fuel for stoichiometric combustion
OCV: Open circuit voltage
P: FFC peak power density
RFQL: Rich-burn, Flame-assisted fuel cell, Quick-mix, Lean-burn
RQL: Rich-burn, Quick-mix, Lean-burn or Rich-Quench-Lean
SDC: Samaria-doped Ceria
SC-SOFC: Single chamber solid oxide fuel cell
SOFC: Solid oxide fuel cell
V_m: Molar volume at standard conditions
$\dot{V}$: Methane flow rate at standard conditions
YSZ: Yttria stabilized zirconia
ε: FFC electrical efficiency